

Cosmological Inference using Gravitational Wave Standard Sirens: A Mock Data Challenge

Rachel Gray,^{1,*} Ignacio Magaña Hernandez,^{2,†} Hong Qi,^{3,‡} Ankan Sur,^{4,5,§} Patrick R. Brady,²
Hsin-Yu Chen,⁶ Will M. Farr,^{7,8} Maya Fishbach,⁹ Jonathan R. Gair,^{10,11} Archisman Ghosh,⁴
Daniel E. Holz,⁹ Simone Mastroianni,¹² Christopher Messenger,¹ Danièle A. Steer,¹² and John Veitch¹

¹*SUPA, University of Glasgow, Glasgow G12 8QQ, United Kingdom*

²*University of Wisconsin-Milwaukee, Milwaukee, WI 53201, USA*

³*Cardiff University, Cardiff CF24 3AA, United Kingdom*

⁴*Nikhef, Science Park 105, 1098 XG Amsterdam, The Netherlands*

⁵*Nicolaus Copernicus Astronomical Center, Polish Academy of Sciences, 00-716, Warsaw, Poland*

⁶*Black Hole Initiative, Harvard University, Cambridge, Massachusetts 02138, USA*

⁷*Department of Physics and Astronomy, Stony Brook University, Stony Brook NY 11794, USA*

⁸*Center for Computational Astronomy, Flatiron Institute, New York NY 10010, USA*

⁹*University of Chicago, Chicago, IL 60637, USA*

¹⁰*School of Mathematics, University of Edinburgh, Edinburgh EH9 3FD, United Kingdom*

¹¹*Max Planck Institute for Gravitational Physics (Albert Einstein Institute), Potsdam-Golm, 14476, Germany*

¹²*AstroParticule et Cosmologie, Université Paris Diderot, F-75205 Paris, France*

(Dated: July 7, 2022)

The detection of gravitational waves from the binary neutron star merger GW170817 alongside its optical counterparts, marked the beginning of gravitational wave cosmology as it allowed for the first constraint on the Hubble constant H_0 using gravitational wave standard sirens. In the upcoming observing run(s) of the Advanced LIGO and Virgo detector network, we expect to detect up to two binary black holes per week and up to one binary neutron star merger per week. It is conceivable that the majority of binary neutron star events will be detected without an optical counterpart, and as such, focus has been on preparing a statistical analysis, in which the distance estimates from binary neutron stars are combined with the redshift data from galaxy catalogs in order to estimate Hubble constant. Thus, we have developed a Bayesian formalism that measures the Hubble constant from gravitational wave events both statistically and with electromagnetic counterparts. To test the formalism on its ability to correctly take into account both gravitational wave and electromagnetic selection effects, a series of mock data challenges were created and analyzed. In this paper, we discuss the assumptions that went into creating the mock data challenges, the method to approach the problem, and the results produced. We show how the incompleteness of galaxy catalogs has an effect on the final measurement of H_0 as well as the effects of weighting each galaxy according to its luminosity.

I. INTRODUCTION

The idea that gravitational waves (GW) detections can be used for the inference of cosmological parameters, such as the Hubble constant (H_0), was first proposed over three decades ago by Bernard Schutz [1]. The key to this process is that GW signals from compact binary coalescences (CBCs) act as standard sirens, in the sense that they provide a self-calibrated luminosity distance to the source. This can be obtained directly from the GW signal, and is therefore entirely independent of the cosmic distance ladder. With the addition of redshift information for each source we then have the required input for cosmological inference.

At the time of writing, the current percent level state-of-the-art electromagnetic (EM) measurements of H_0 are in tension with each other. The Planck experiment uses measurements of cosmic microwave background (CMB) anisotropies and provides a value of $H_0 = 67.4 \pm 0.5 \text{ km s}^{-1} \text{ Mpc}^{-1}$ [2]. The Supernovae, H_0 , for the Equation of State of Dark en-

ergy (SHOES) experiment measures distances to Type Ia supernovae standard candles making use of the cosmic distance ladder, and gives $H_0 = 74.03 \pm 1.42 \text{ km s}^{-1} \text{ Mpc}^{-1}$ [3]. These two independent measurements of H_0 are in tension at the level of $\sim 4.4\text{-}\sigma$ [3]. Add H0LICOW strong lensing tests and the tip of the red giant branch measurement maybe?.

This indicates the possibility that one (or both) of these measurements is subject to unknown systematics, or whether it could be an indication of new physics causing the discrepancy between the local measurements and the non-local (early universe) CMB based measurement. This makes a GW standard siren measurement of H_0 particularly interesting, as this will provide a local constraint on H_0 which is entirely independent of the cosmic distance ladder. In this manner, the use of GWs as standard sirens may allow us to arbitrate the current situation, indicating either a bias in the current measurements, or pointing towards new physics.

The detection of the binary neutron star (BNS) event GW170817 [4], together with its optical counterpart [5, 6] led to the first standard siren measurement of H_0 [7]. The counterpart associated with GW170817 allowed for the identification of its host galaxy, NGC4993, and hence a direct measurement of its redshift, which in turn resulted in the inferred value $H_0 = 70_{-8}^{+12} \text{ km s}^{-1} \text{ Mpc}^{-1}$.

Central to the aims of this paper, is the case where an EM counterpart is not observed, and how H_0 inference can still be

* rachel.gray@ligo.org

† ignacio.magana@ligo.org

‡ hong.qi@ligo.org

§ ankan.sur@ligo.org

performed. In particular, the method proposed by Schutz in 1986 [1, 8] allows the use of galaxy catalogs to provide redshift information for potential host galaxies within the event’s GW sky-localization. The idea is that, by marginalising over the possible discrete values of redshift for each GW detection we account for uncertainty as to which galaxy is the true host. By combining the information from many GW events, the contributions from the true host galaxies will grow since they will all share the same true H_0 . Contributions from the others will statistically average out, leading to a constraint on H_0 and possibly other cosmological parameters.

Over the course of the first observing run (O1) and the second observing run (O2) a total of 11 GW events were detected by the advanced LIGO and Virgo detectors: 10 are binary black hole (BBH) events and one is a BNS event [9]. The “galaxy catalog” method has been independently applied to both the BNS event GW170817 (without assuming NGC4993 is the host) [10], and the BBH event GW170814 [11] resulting in posterior probability distributions on H_0 where the posterior from GW170814 was broader than (but consistent with) that obtained from GW170817. The difference in the widths of the H_0 constraints is an expected result due to the larger localisation volume associated with GW170814, and the high number of galaxies it contained. Using the detections from O1 and O2, for the first time, multiple GW events have been combined to give the latest standard siren measurement of H_0 [12] using the methodology presented in this paper.

Predictions suggest that it will be possible to constrain H_0 to less than 2% within 5 years of the start of the third observing run (O3) and to 1% within a decade, though this is dependent on the number of events observed with EM counterparts [13], and may change as our understanding of astrophysical rates improves. This prediction also relies on future GW observatories joining the network to further improve event sky-localization [14]. With the Japanese detector KAGRA set to join late in 2019 [15] and LIGO-India approved for construction [16], the next decade of standard siren cosmology is set to be very exciting.

O3 began on April 1st 2019 and will last for one full year. The sensitivities of the LIGO and Virgo detectors have improved since O2, leading to an increased detection rate of GW candidates¹ [17]. This is the first observing run for which there will be 3 detectors operating for the entirety of the run. More detectors improve the duty-cycle (the fraction of time that 1 or more detectors is online) of the network, it also increases the rate of three-detector detections, which will likely be better localized on the sky than those only detected by two detectors. This is important, both in terms of performing EM follow-up for EM counterparts practically [18], and for reducing the number of possible host galaxies for events in the case where a counterpart is not observed.

This paper presents the Bayesian framework behind the

gwcsmo code, a product of the LIGO and Virgo Collaboration (LVC) which was used to measure H_0 using detected GW events from O1 and O2 [12], and will be used to analyse events from O3 and beyond. We present results from a series of mock data challenges (MDCs) which were designed specifically to test this method’s robustness against some of the most common pitfalls, in particular GW selection effects present in identifying detections and EM selection effects governing the content of galaxy catalogues. This method builds upon the Bayesian framework first presented in [8] which has subsequently been extended, modified and independently derived by multiple authors [11, 13, 19]. With specific care regarding selection effects we outline methods for constraining H_0 using both the “galaxy catalog” and “EM counterpart” approaches.

This paper is structured as follows. Section II presents the Bayesian framework used to estimate the posterior on H_0 . Section III discusses the design and preparation of the MDCs and in Section IV we present our results. We conclude in Section V giving a detailed discussion of results and providing guidance for future work. Some of the details of the Bayesian method have been set aside to be discussed in an Appendix.

II. METHODOLOGY

The late-time cosmological expansion in a Friedmann-Lemaître-Robertson-Walker universe is characterized by the Hubble parameter as a function of the redshift z ,

$$H(z) = H_0 \sqrt{\Omega_m(1+z)^3 + \Omega_k(1+z)^2 + \Omega_\Lambda}, \quad (1)$$

where H_0 is the Hubble constant, the rate of expansion in the current epoch, and Ω_m and Ω_Λ are the fractional matter density (including baryonic and cold dark matter) and fractional dark energy density (assumed to be due to a cosmological constant) respectively; Ω_k is the fractional curvature energy density which is identically zero for a “flat” universe consistent with observations. Additionally, we have the constraint $\Omega_m + \Omega_k + \Omega_\Lambda = 1$ for all the components contributing to the energy density of universe at the present epoch.

The expansion history of the universe maps to a “redshift-distance relation” associating the redshift z of observable sources to their luminosity distance $d_L(z)$ (see *e.g.* [20]) as,

$$d_L(z) = \frac{c(1+z)}{H_0} \int_0^z \frac{H_0}{H(z')} dz'. \quad (2)$$

From the relation between observed z and d_L to sources (EM sources such as variable stars or supernovae, or GW sources), one can measure the cosmological parameters appearing in $H(z)$. With knowledge of the other cosmological parameters $\{\Omega_m, \Omega_k, \Omega_\Lambda\}$ coming from independent observations, the redshift-distance relation can be used to measure H_0 . We would like to note that with prior knowledge on the other cosmological parameters coming from EM observations, the measurement made with GW detections are not strictly independent measurements.

At low redshifts $z \ll 1$, the redshift-distance relation can be approximately described by the linear Hubble relation,

$$d_L(z) \approx cz/H_0, \quad (3)$$

¹ At present in O3 the detectors appear to be averaging the detection of one GW candidate per week. If all of these candidates are ultimately identified as real GW events, then O3 within its first two months will have exceeded the total number of detections of O1 and O2.

which contains H_0 but is independent of the other cosmological parameters. With this approximate linear relation at low redshifts, any measurement of H_0 with GWs is independent of the values of the other cosmological parameters.

A. Standard Sirens

The amplitude of the observed strain is inversely proportional to the luminosity distance to the GW source. For compact binary sources, to the leading order (see, *e.g.* [21]),

$$A \sim \frac{\mathcal{M}_z^{5/3}}{d_L} [f(\mathcal{M}_z, t)]^{2/3}, \quad (4)$$

where A is the observed amplitude, $\mathcal{M}_z \equiv \mathcal{M}(1+z)$ is the detector frame ‘‘chirp’’ mass (redshifted relative to its source frame value \mathcal{M}), and $f(\mathcal{M}_z, t)$ is the evolution of the observed frequency. \mathcal{M}_z can be estimated from the observed $f(\mathcal{M}_z, t)$. The luminosity distance, d_L , can then be obtained directly from the amplitude of signal. This makes compact binaries self-calibrated luminosity distance indicators or ‘‘standard sirens’’ unlike EM distance indicators which need to undergo calibration via multiple rungs of the cosmic distance ladder. The redshift of the GW source, also required for cosmological inference, however remains degenerate with the source’s mass, contained within \mathcal{M}_z , and needs to be estimated in alternate ways.

B. Galaxy Information

There are multiple ways in which EM observations can provide complementary redshift². A BNS event may be detected in coincidence with an EM counterpart, which can be associated with the host galaxy to provide a direct measurement of the redshift of the source. More generically, a GW event may not have a detected EM counterpart, in which case one needs to fall back on the method outlined by Schutz [1] and use potential host galaxies within the event’s sky localization region for the redshift information for the source. Two possibilities come up: (i) to use available galaxy catalogs, or (ii) to conduct dedicated EM follow-up on the event’s sky region, mapping the galaxies within that area to as great a depth as possible to maximize the redshift information available.

While using galaxy catalogs to provide the prior redshift information, the possibility that the host galaxy lies beyond the reach of the catalog must be taken into account. EM telescopes are flux limited, and can be reasonably modeled as having an apparent magnitude limit. This means that galaxy catalogs are inherently biased towards containing objects which are brighter and/or nearer-by. These EM selection effects must be compensated for. Carrying out dedicated EM follow-up

will, to some degree, mitigate this issue, as it will allow for far deeper coverage over a small section of the sky. For nearby events, the possibility that the host galaxy lies beyond the telescope’s sight may be negligible. However, the time and resources required for dedicated EM follow-up means that the default approach for GW events observed without counterparts will be to use pre-existing catalogs.

In either case, the uncertainty associated with each galaxy’s redshift must be taken into account, including the redshift error due to the galaxy’s peculiar velocity, v_p . This is especially true for nearby galaxies, for which this contribution will dominate. The effect of v_p on the measurement of H_0 may be small if there are a large number of potential host galaxies in the GW events sky-localization, but for a small number of galaxies, and for the counterpart case in particular, this effect is particularly noticeable (see the treatment in [7]).

C. Bayesian Framework

The posterior probability on H_0 from N_{det} GW events is computed as follows:

$$p(H_0|\{x_{\text{GW}}\}, \{D_{\text{GW}}\}) \propto p(H_0)p(N_{\text{det}}|H_0) \prod_i^{N_{\text{det}}} p(x_{\text{GW}i}|D_{\text{GW}i}, H_0) \quad (5)$$

where $\{x_{\text{GW}}\}$ is the set of GW data, D_{GW} indicates that the event was detected as a GW and $p(H_0)$ is the prior on H_0 . For a given H_0 , the term $p(N_{\text{det}}|H_0)$ is the likelihood of detecting N_{det} events. It depends on the intrinsic astrophysical rate of events in the source frame, $R = \frac{\partial N}{\partial V \partial T}$. The total number of expected events is given by $N_{\text{det}} = R \langle VT \rangle$, where $\langle VT \rangle$ is the average of the comoving volume multiplied by the observation time. By choosing a ‘‘non-informative’’ prior on rate, $p(R) \propto 1/R$, the dependence on H_0 drops out [24]. For simplicity this approximation is made throughout the analysis.

The remaining term factorizes into likelihoods for each detected event, using Bayes theorem we can write it as,

$$\begin{aligned} p(x_{\text{GW}}|D_{\text{GW}}, H_0) &= \frac{p(D_{\text{GW}}|x_{\text{GW}}, H_0)p(x_{\text{GW}}|H_0)}{p(D_{\text{GW}}|H_0)} \\ &= \frac{p(x_{\text{GW}}|H_0)}{p(D_{\text{GW}}|H_0)}, \end{aligned} \quad (6)$$

where we set $p(D_{\text{GW}}|x_{\text{GW}}, H_0) = 1$, since the analysis is only carried out when the signal-to-noise ratio (SNR), ρ , associated with x_{GW} passes some detection statistic threshold ρ_{th} – it is a prerequisite that the event has been detected. Calculating $p(D_{\text{GW}}|H_0)$ requires integrating over all possible realizations of GW events, with a lower integration limit of ρ_{th} :

$$p(D_{\text{GW}}|H_0) = \int_{\rho > \rho_{\text{th}}}^{\infty} p(x_{\text{GW}}|H_0) dx_{\text{GW}}. \quad (7)$$

For explicit details on the calculation of $p(D_{\text{GW}}|H_0)$ see Appendix 5.

² There are ways of obtaining the redshift independent of EM observations, by using known BNS population properties such as the mass distribution [22], or the neutron star equation-of-state [23].

1. The galaxy catalog method

In the galaxy catalog case, the EM information enters the analysis as a prior, made up of a series of possibly smoothed delta functions³ at the redshift, right ascension (RA) and declination (dec) of the possible source locations. As we are in the regime where (especially for BBHs) galaxy catalogs cannot be considered complete out to the distances to which GW events are detectable, we have to consider the possibility that the host galaxy is not contained within the galaxy catalog, but lies somewhere beyond it. In order to do so, we marginalize the likelihood over the case where the host galaxy is, and is not, in the catalog (denoted by G and \bar{G} respectively):

$$p(x_{\text{GW}}|D_{\text{GW}}, H_0) = \sum_{g=G, \bar{G}} p(x_{\text{GW}}|g, D_{\text{GW}}, H_0)p(g|D_{\text{GW}}, H_0). \quad (8)$$

We defer detailed derivations for each of the components of Eq. (8) to Appendix 2.

2. The counterpart method

The method outlined above is for the statistical galaxy catalog case, in which no EM counterpart is observed, or expected. We also consider the case where we observe an EM counterpart. The main difference is the inclusion of a likelihood term for the EM counterpart data, mirroring that of the GW data.

The likelihood in this case (term within the product in Eq. 5) is given by:

$$\begin{aligned} & p(x_{\text{GW}}, x_{\text{EM}}|D_{\text{GW}}, D_{\text{EM}}, H_0) \\ &= \frac{p(x_{\text{GW}}, x_{\text{EM}}|H_0)p(D_{\text{GW}}, D_{\text{EM}}|x_{\text{GW}}, x_{\text{EM}}, H_0)}{p(D_{\text{GW}}, D_{\text{EM}}|H_0)}, \\ &= \frac{p(x_{\text{GW}}|H_0)p(x_{\text{EM}}|H_0)}{p(D_{\text{EM}}|D_{\text{GW}}, H_0)p(D_{\text{GW}}|H_0)}, \\ &\propto \frac{p(x_{\text{GW}}|H_0)p(x_{\text{EM}}|H_0)}{p(D_{\text{GW}}|H_0)}. \end{aligned} \quad (9)$$

where in the numerator we have assumed that the GW and EM data are independent of each other and so the joint GW-EM likelihood factors out. $p(D_{\text{GW}}, D_{\text{EM}}|x_{\text{GW}}, x_{\text{EM}}, H_0) = 1$ whenever we have GW and EM data. We make the assumption that the detection of an EM counterpart is also flux-limited, and hence also dependent on the luminosity distance (as opposed to the redshift). Since both D_{GW} and D_{EM} are functions of only the luminosity distance, the term $p(D_{\text{EM}}|D_{\text{GW}}, H_0)$ is then some constant independent of H_0 .

In an ideal scenario, the observation of an EM counterpart will allow for the identification of one of the galaxies in the neighboring region as the host of the GW event. In the case where the EM counterpart cannot be unambiguously linked to a host galaxy, this uncertainty can also be taken into account. See Appendix 4 for more details.

³ While uncertainties on the galaxy sky-coordinates can be safely ignored, the error on the redshift can be modeled with a Gaussian or a more complicated distribution.

III. THE MOCK DATA CHALLENGE

In this section we describe a series of mock data challenges (MDCs) that we use to test the Bayesian formalism described in Section II and their ability to infer the posterior on H_0 under different conditions. For each case, the MDC consists of (i) simulated GW data, and (ii) a corresponding mock galaxy catalog.

For each of the MDCs we use an identical set of simulated BNS events from The First Two Years of Electromagnetic Follow-Up with Advanced LIGO and Virgo dataset [25, 26]⁴. The set of BNS events comes from an end-to-end simulation of approximately 50,000 “injected” events in detector noise corresponding to a sensitivity similar to what was achieved during O2. Only a subset (approximately 500 events) were “detected” by a network of two or three detectors with the GstLAL matched filter based detection pipeline [27]. From the above detections, 249 events were randomly selected (in a way that no selection bias was introduced), and these events underwent full Bayesian parameter estimation using the LALInference software library [28] to obtain gravitational wave posterior samples and skymaps. Consistency the First Two Years parameter estimation results in terms of sky localization areas and 3D volumes was demonstrated in [29]. It is these 249 events of the First Two Years dataset and the associated GW data which we use for our analysis.

The galaxy catalogs for each iteration of the MDC described below are designed to test a new part of the gwcosmo methodology in a cumulative fashion, starting with GW selection effects, adding in EM selection effects, and finally testing the ability to utilize the information available in the observed brightness of host galaxies, by weighting the galaxies with a function of their intrinsic luminosities.

The starting point for the galaxy catalogs is to take all 50,000 injected events from the First Two Years dataset and simulate a mock universe, which contain a galaxy corresponding to each injected event’s sky location and luminosity distance, where the latter is converted to a redshift using a fiducial “injected” H_0 value of $70 \text{ km s}^{-1} \text{ Mpc}^{-1}$. The First Two Years data was originally simulated in a universe where GW events followed a d_L^2 distribution, and there was no distinction between the source frame and the (redshifted) detector frame masses. Though not ideal, this data reasonably mimics a low redshift universe ($z \ll 1$) in which the linear Hubble relation of Eq. 3 holds, and galaxies follow a z^2 distribution. We use the same linear relation for the generation of the MDC universe (*i.e.* a set of simulated galaxy catalog parameters) for each of the MDCs. It should be emphasized that the Bayesian method for estimation of H_0 outlined in Section II above is general, and can be extended to realistic scenarios with a non-

⁴ The set of simulations in [26] are more realistic with the same injections in (recolored) detector data as opposed to Gaussian noise used in [25]. Correspondingly, the detection criterion is in terms of a false alarm rate (FAR) rather than a threshold on the SNR. This is an important distinction, particularly affecting events marginally close to the detection threshold. We use the simplified set of simulations in [25] noting potential caveats.

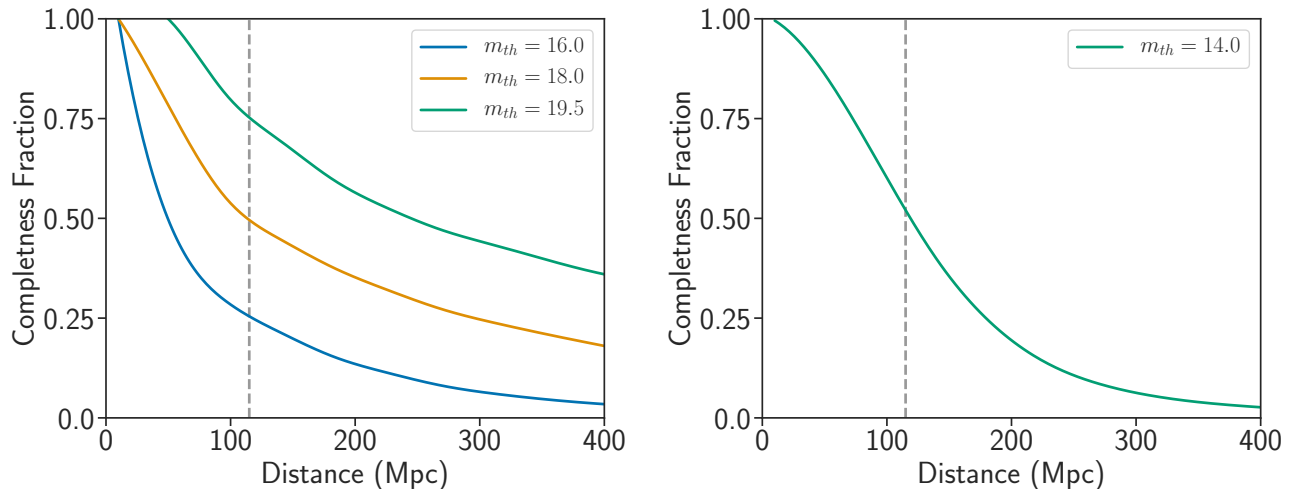


FIG. 1. Galaxy catalog completeness fractions for MDC2 and MDC3. *Left panel:* Galaxy number completeness fraction defined in Eq. (11) as a function of luminosity distance for the three MDC2 sub-catalogs. The lines in blue, orange and green correspond to the catalogs with $m_{th} = 16, 18,$ and 19.5 respectively; these correspond to completeness fractions of 25%, 50% and 75% out to a fiducial reference distance of 115 Mpc (shown as a vertical grey line). *Right panel:* The galaxy luminosity completeness fraction defined in Eq. (15) as a function of luminosity distance for the MDC3 catalog, with $m_{th} = 14$. At the reference distance of 115 Mpc (vertical grey line), this corresponds to a completeness fraction of $\sim 50\%$.

linear cosmology with $\{\Omega_m, \Omega_k, \Omega_\Lambda\}$ held fixed. So, in particular, the method is applicable for events which are detected at higher distances, where low redshift approximation breaks down. The restriction to a linear cosmology in this paper comes only due to the use of the MDC dataset. We would like to note that by using a linear cosmology, we are not testing possible effects introduced by the presence of other cosmological parameters. The statistical analysis at large redshifts would, for example, be sensitive to the values (or the assumed prior ranges) of the parameters like Ω_m and Ω_Λ .

The first few columns of Table I summarize the characteristics of each of the galaxy catalogs created and how they correspond to each MDC. We give a brief description for each of the cases below.

A. MDC0: Known Associated Host Galaxies

MDC0 is the simplest version of the direct counterpart case, in which we identify with certainty the host galaxy for each GW event. As the galaxies are generated with no redshift uncertainties or peculiar velocities, these results will be (very) optimistic for the counterpart case. Analysis of this MDC provides the “best possible” constraint on H_0 using the 249 events, which then allows for comparison with the other MDCs.

B. MDC1: Complete Galaxy Catalog

The MDC1 universe consists of the full set of 50,000 galaxies out to $z \approx 0.1$ ($d_L \approx 428$ Mpc) in the original First Two

Years dataset. This gives a galaxy number density of ~ 1 per 7000 Mpc^3 , which is ~ 35 times sparse compared to the actual density of galaxies in the local universe [30]. Additional galaxies are generated beyond the edge of the dataset universe, uniformly across the sky and uniformly in comoving volume, thereby extending the universe out to a radius of 2000 Mpc ($z = 0.467$ for $H_0 = 70 \text{ km s}^{-1} \text{ Mpc}^{-1}$). This means that, even allowing H_0 to be as large as $200 \text{ km s}^{-1} \text{ Mpc}^{-1}$, the edge of the MDC universe is more than twice the highest redshift associated with the farthest detection (which is at $\sim 270 \text{ Mpc}$)⁵. Each of the 249 detected BNS have a unique associated host galaxy contained within the MDC1 catalog. This catalog is thus *complete* in the sense that it contains every galaxy in the simulated universe. We refer to the MDC universe as MDC1 throughout the rest of the paper, and similarly for the subsequent MDCs.

MDC1 is designed to further test the GW selection effects by ensuring that, given a set of sources and access to a complete catalog, our methodology and analysis produces a result consistent with the simulated value of H_0 .

C. MDC2: Incomplete Galaxy Catalog

MDC2 is designed to test EM selection effects, by applying an apparent magnitude threshold to the MDC universe, such that a certain fraction of the host galaxies is not contained in it. This is a necessary consideration, given that we are in the

⁵ For MDC1 and for all subsequent MDCs, it has been tested that the artificial “edge of the universe” has no bearing on the results.

regime where GW signals are being detected beyond the distance to which the current galaxy catalogs can be considered to be complete. This has been true for BBHs detections since O1, and is true of BNSs as well now we are in O3.

In order to create the catalog for MDC2, we start with the initial MDC1 universe and assign luminosities to each of the galaxies within it. We assume a luminosity distribution that follows a Schechter function of the form (see *e.g.* [31])

$$\phi(L) dL = n^* \left(\frac{L}{L^*} \right)^\alpha e^{-L/L^*} \frac{dL}{L^*}, \quad (10)$$

where L denotes a given galaxy luminosity and $\phi(L) dL$ is the number of galaxies within the luminosity interval $[L, L + dL]$. The characteristic galaxy luminosity is given by $L^* = 1.2 \times 10^{10} h^{-2} L_\odot$ with solar luminosity $L_\odot = 3.828 \times 10^{26}$ W, and $h \equiv H_0 / (100 \text{ km s}^{-1} \text{ Mpc}^{-1})^6$, $\alpha = -1.07$ characterizes the exponential drop off of the luminosity function, and n^* denotes the number density of objects in the MDC universe (in practice, this only acts as a normalization constant). The integral of the Schechter function diverges at $L \rightarrow 0$, requiring a lower luminosity cut off for the dimmest galaxies in the universe which we set to $L_{\text{lower}} = 0.001 L^*$. This choice is arbitrary for our purpose here, but small enough to include almost all objects classified as galaxies in real catalogs like GLADE [30].

These luminosities are then converted to apparent magnitudes using $m \equiv 25 - 2.5 \log_{10}(L/L^*) + 5 \log_{10}(d_L/\text{Mpc})$, and an apparent magnitude threshold m_{th} is applied as a very crude characterization of the selection function of an optical telescope observing only objects with $m < m_{\text{th}}$. MDC2 is broken into three sub-MDCs, in order to test our ability to handle different levels of galaxy catalog completeness dictated by different telescope sensitivity thresholds. In each case, the catalog completeness is defined as the ratio of the number of galaxies inside the catalog relative to the number of galaxies inside the MDC universe, out to a reference fiducial distance d_L ,

$$f_{\text{completeness}}(d_L) = \frac{\sum_j^{\text{MDC2}}(d_{L_j} < d_L)}{\sum_k^{\text{MDC1}}(d_{L_k} < d_L)}, \quad (11)$$

where the numerator is a sum over the galaxies contained within the MDC2 catalog out to some reference distance d_L , and the denominator is a sum over the galaxies in the MDC1 catalog.

Apparent magnitude thresholds of $m_{\text{th}} = 19.5, 18,$ and 16 are chosen for the three sub-MDCs, which correspond to cumulative number completeness fractions of 75%, 50% and 25% respectively, evaluated at a distance of $d_L = 115$ Mpc, chosen such that given the luminosity distance distribution of detected BNSs, the completeness fraction for the sub-MDC to this distance is roughly indicative of the percentage of host galaxies which remain inside the galaxy catalog. The left panel of Fig. 1 shows how the completeness of each of the MDC2 catalogs drop off as a function of distance.

⁶ We note that the parameter L^* of the Schechter luminosity function itself depends on H_0 , which we allow to vary and hence take into account within our formalism.

D. MDC3: Luminosity Weighting

MDC3 is designed to test the effect of weighting of galaxies with a function of their luminosity. It is likely that the more luminous galaxies are also more likely hosts for compact binary mergers; the luminosity in blue (B-band) is expected to be indicative of a galaxy's star formation rate, for example, while the luminosity in high infrared (K-band) a tracer of the stellar mass. The bulk of the host probability is expected to be contained within a smaller number of brighter galaxies, effectively reducing the number of galaxies which need to be considered. Additional information from luminosity is thus expected to improve the constraint on H_0 by narrowing its posterior probability density.

For MDC3, the probability of a galaxy emitting a GW signal is taken to be proportional to the galaxy's luminosity. As with MDC2, the luminosity distribution of the galaxies in the universe is assumed to follow the Schechter luminosity function as in Eq. (10) (referred to from now on as $p(L)$). However, the joint probability of a single galaxy having luminosity L and containing an emitting source, s , is

$$p(L, s) = p(s|L) p(L) \propto L p(L), \quad (12)$$

where we assume that the probability of a galaxy of luminosity L hosting a source is proportional to the luminosity itself⁷. All host galaxies thus have luminosities sampled from $L p(L)$. In this context, we must consider all galaxies which emitted signals, not just those which were detected. With this in mind, the overall luminosity distribution has the following form:

$$p(L) = \beta \frac{L}{\langle L \rangle} p(L) + (1 - \beta) x(L) \quad (13)$$

where β is the fraction of emitting galaxies to total galaxies over the observed time period ($1 \geq \beta \geq 0$), $L/\langle L \rangle$ is the normalized luminosity, and $x(L)$ is the unknown luminosity distribution of galaxies which did not emit gravitational waves which we can sample for a given value of β .

Rearranging to obtain the only unknown, $x(L)$, gives

$$x(L) = \frac{p(L)}{1 - \beta} \left[1 - \beta \frac{L}{\langle L \rangle} \right], \quad (14)$$

and from this we see there is an additional constraint on β , because the term inside the brackets must be > 0 . The maximum value that β can take is given by $\beta_{\text{max}} = \langle L \rangle / L_{\text{max}}$, where L_{max} is the maximum luminosity from the Schechter function, and $\langle L \rangle$ is the mean. From the Schechter function parameters detailed in section III C, $\beta_{\text{max}} \approx 0.015$.

⁷ Luminosity weighting is motivated by the expectation the brighter galaxies are more likely hosts. Here we assume a linear relation between luminosity of a galaxy and its probability of hosting a source. Luminosities in the B- or K-bands, respectively indicative of galaxies' star formation rate or stellar mass, for example, may be expected to be approximately proportional to their probability of hosting compact binary sources.

We recall that the original First Two Years data was generated by simulating $\sim 50,000$ BNS events, of which ~ 500 were detected, of which 249 randomly selected detections underwent parameter estimation. The number of “emitting” and “non-emitting” galaxies have to be re-scaled to represent that. Approximately half of the original events are chosen to be “emitters”, including the 249 detected ones. With this in mind, luminosities can not be assigned to their host galaxies without adding a greater density of non-emitting galaxies in order to satisfy the requirements for β . Thus for MDC3, the density of galaxies is increased by a factor of 100, with the acknowledgement that this would lead to a broadening of the final posterior. This means that MDC3 is not directly comparable with the previous MDC versions. The galaxies which are considered “emitters” are assigned luminosities from $L_p(L)$, and “non-emitters” from $x(L)$ above.

In order to include EM selection effects, an apparent magnitude cut m_{th} of 14 is applied, such that the completeness of the galaxy catalog is $\sim 50\%$ out to the same fiducial distance of 115 Mpc as in MDC2. In this case, completeness is however defined in terms of the fractional luminosity contained in the catalog, rather than in terms of numbers of objects:

$$f_{\text{completeness}}(d_L) = \frac{\sum_j^{\text{MDC3}} L_j(d_{L_j} < d_L)}{\sum_k^{\text{complete}} L_k(d_{L_k} < d_L)}, \quad (15)$$

where the numerator is summed over the galaxies inside the MDC3 apparent magnitude-limited catalog, and the denominator is summed over the galaxies in the whole MDC3 universe. This is shown in the right panel of Fig. 1. As the emitting galaxies are luminosity weighted, the cumulative luminosity completeness is representative of the percentage of BNS events inside the catalog.

IV. RESULTS

In this section we summarize the results for the mock data challenges described in Section III. We show the combined posteriors on H_0 for each MDC, discuss the convergence to the simulated value of $H_0 = 70 \text{ km s}^{-1} \text{ Mpc}^{-1}$ and calculate the expected precision of the combined measurement under each set of conditions. In Table I we list the measured values of the Hubble constant for the combined 249 event posterior (maximum a posteriori and 68.3% highest density posterior intervals) all computed with a uniform prior in the range of $[20, 200] \text{ km s}^{-1} \text{ Mpc}^{-1}$, as well as the corresponding fractional uncertainties for each of the MDCs.

A. MDC0: Known Associated Host Galaxies

We first consider the simple case where we identify the true host galaxy for every event and determine the resulting 249-event combined H_0 posterior. Fig. 2 presents the results of this analysis. The likelihoods for each individual GW event are shown (each is normalised but scaled up for clarity) shaded by the event’s optimal SNR. In this case, of known counterpart,

the likelihoods are informative, having a clearly-defined peak corresponding to finding the likely values of H_0 for the known galaxy redshift, and the clearly-peaked d_L distribution for the event. This distribution usually has a single peak, but in some circumstances there can be two or more [25, 26]. We see that the peaks of the individual likelihoods do not necessarily correspond to the true value $H_0 = 70 \text{ km s}^{-1} \text{ Mpc}^{-1}$, but there is always support for it. Therefore it is the only consistent value for all events, driving the combined posterior, which is overlaid in orange. This gives us a statistical estimate for the maximum a-posteriori value and 68.3% maximum-density credible interval for H_0 as $69.08^{+0.79}_{-0.80} \text{ km s}^{-1} \text{ Mpc}^{-1}$. In combining all the events, we see that the final result is well-converged toward a symmetric Gaussian distribution.

The result of MDC0 provides us with the best possible H_0 estimate given this set of GW detections, as this case corresponds to perfect knowledge of the host galaxy. This gives us a good benchmark against which other versions of the MDC can be compared.

Since this is a best-case scenario, we have the least statistical uncertainty in the final result, making any systematic bias more apparent than for the later MDCs. For the final result with 249 events, the true value is contained within the posterior. Therefore we are confident that our method is free of systematics to the required level for BNS counterpart measurements in observing runs in the Advanced-detector era.

B. MDC1: Complete Galaxy Catalog

The next most complex case is MDC1, where we assume no counterpart was observed, and resort to using a galaxy catalog. However, MDC1 uses a *complete* galaxy catalog, so contains all potential hosts, and so EM selection effects are not present yet. Although this is an artificially optimistic scenario, we see that MDC1 already produces a wider posterior on H_0 ($68.91^{+1.36}_{-1.22} \text{ km s}^{-1} \text{ Mpc}^{-1}$) than MDC0, because of the uncertainty of the host galaxy, shown in Fig. 3. The introduction of this uncertainty means that the contributions from each event will be smoothed out, depending on the size of the event’s sky localization and the number of galaxies within it. As can be seen in Fig. 4, there is a far higher proportion of events for which the posterior is relatively broad and less informative, in comparison to Fig. 2. However, many events clearly have a small number of galaxies in their sky-area, and hence still show clear peaks.

MDC1 additionally demonstrates the importance of correctly accounting for GW selection effects. We are biased towards detecting sources which are nearer-by, and which are optimally orientated (closer to face-on). If an analysis is performed without taking into consideration the denominator $p(D_{\text{GW}}|H_0)$ of Eq. (6), that corrects for the above GW selection effects, the posterior density on H_0 converges to a value different from its injected value of $70 \text{ km s}^{-1} \text{ Mpc}^{-1}$.

MDC	Host galaxy preference	Completeness ^a	m_{th}	Analysis assumption	H_0 (km s ⁻¹ Mpc ⁻¹)	Percentage Error
0	Known host	-	-	direct counterpart	$69.08^{+0.79}_{-0.80}$	1.13%
1	equal weights	100%	-	unweighted catalog	$68.91^{+1.36}_{-1.22}$	1.84%
2a	equal weights	75%	19.5	unweighted catalog	$69.69^{+1.66}_{-1.44}$	2.21%
2b	equal weights	50%	18	unweighted catalog	$69.76^{+1.79}_{-1.65}$	2.46%
2c	equal weights	25%	unweighted catalog	$69.64^{+2.44}_{-2.10}$	3.24%	
3a	luminosity weighted	50%	14	weighted catalog	$70.38^{+3.49}_{-2.64}$	4.38%
3b	luminosity weighted	50%	14	unweighted catalog	$68.95^{+4.41}_{-3.54}$	5.68%

^a The completeness is calculated as a number completeness using Eq. (11) for MDCs 1 and 2, and as a luminosity completeness using Eq. (15) for MDC 3, out to a fiducial distance of 115 Mpc, such that it is indicative of the fraction of host galaxies which are inside the galaxy catalog in both cases.

TABLE I. A summary of the main results from each of the MDCs. For H_0 we quote the mode and the 68.3% error region values with their 1 σ error. The percentage error in H_0 is defined as the half-width of the 68.3% highest probability interval divided by 70 km s⁻¹ Mpc⁻¹.

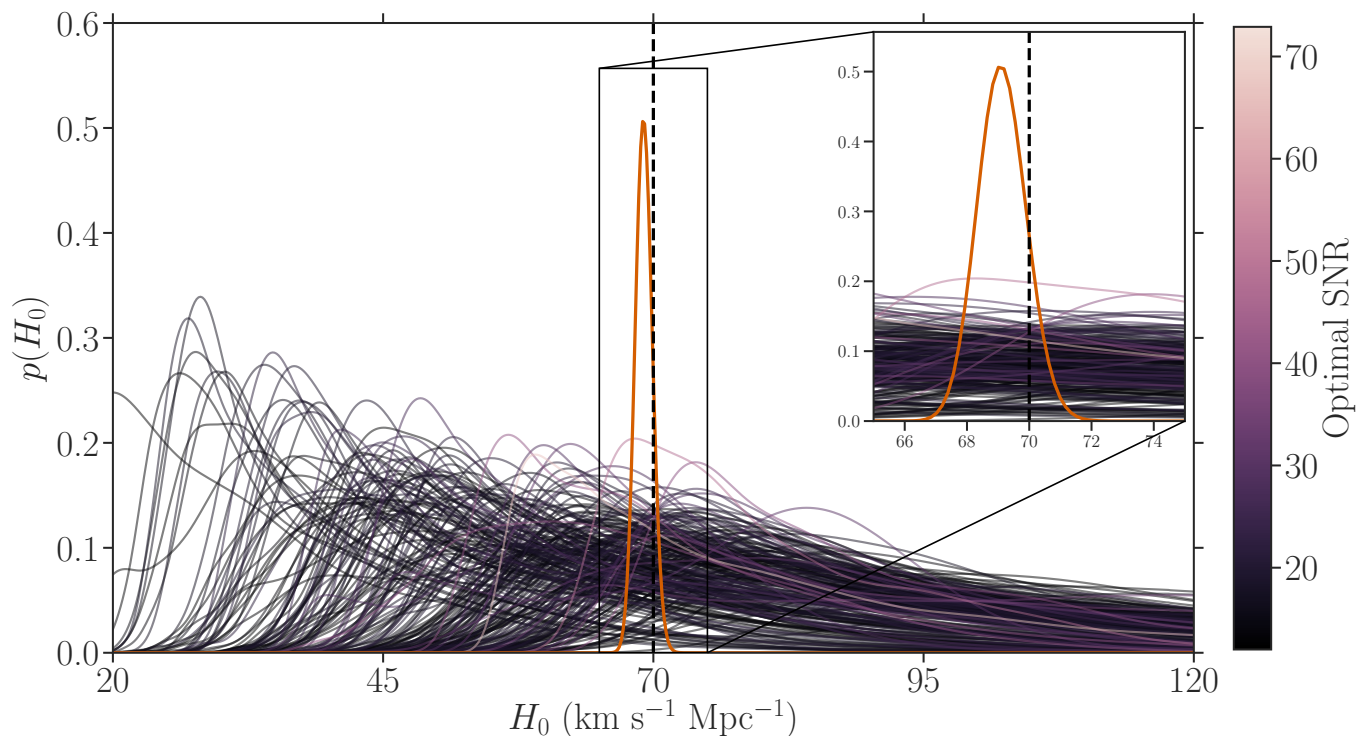


FIG. 2. In orange we show the posterior probability on H_0 for MDC0. We also show the individual likelihoods of all events, color coded according to their optimal SNR, and scaled up by an arbitrary value for easier viewing.

C. MDC2: Incomplete Galaxy Catalog

The next most complex scenario is the case where we have incomplete galaxy catalogs, limited by an apparent magnitude threshold. This gives us the first case where accounting for EM selection effects is important. To investigate this, we consider three galaxy catalogs, with apparent magnitude thresholds of 16, 18 and 19.5, with respective completeness fractions of 25%, 50% and 75% (see III C for details). The combined 249-event posterior distributions on H_0 are shown

in Fig. 5.

As the catalogs become less complete (as defined by Eq. (11)), the combined H_0 posterior becomes wider. This is because the probability that the host galaxy is inside the catalog decreases. The contribution from the galaxies within the catalog is reduced, and the uninformative contribution from the out-of-catalog term in Eq. 8 increases. This is visible in the individual likelihoods shown in Fig. 6, where instead of decreasing toward zero at high values of H_0 , the individual likelihoods tend toward a constant. This is because, in the absence of EM data, and with the linear Hubble relation assumed in

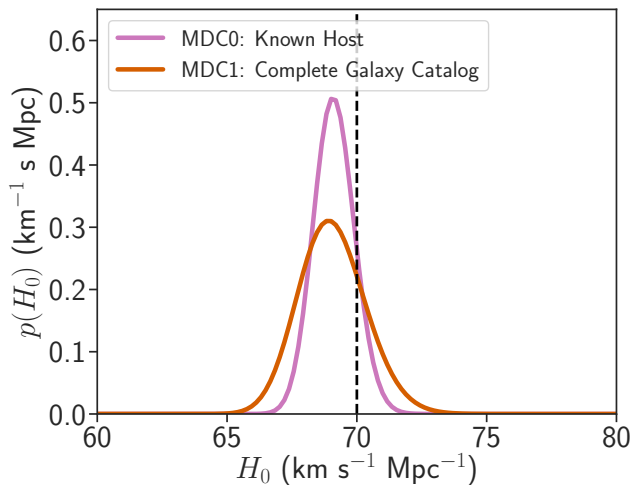


FIG. 3. We show the joint posterior probability on H_0 using all 249 events for MDC0 and MDC1. In purple we show the joint posterior on H_0 for the case where we have identified each events' host galaxy (the direct counterpart case). In red we show the joint posterior on H_0 for the case where we use a complete galaxy catalog.

this work, the number of unobserved galaxies increases without limit as d_L^2 .

For the 25% complete case we estimate H_0 as $69.64^{+2.44}_{-2.10}$ $\text{km s}^{-1} \text{Mpc}^{-1}$, for 50% completeness we find $69.76^{+1.79}_{-1.65}$ $\text{km s}^{-1} \text{Mpc}^{-1}$ and for 75% completeness we find $69.69^{+1.66}_{-1.44}$, all with a uniform prior on the range $[20, 200]$ $\text{km s}^{-1} \text{Mpc}^{-1}$. See section IV E for a more in depth comparison of how galaxy catalog completeness affects posterior width.

For any of the MDC2 catalogs, if we assume that the galaxy catalog is complete, when in reality it is not, we get a posterior on H_0 which is inconsistent with a value of $70 \text{ km s}^{-1} \text{Mpc}^{-1}$. The decisive ruling out of the correct H_0 value tends to be driven by the most well-localized events for which the host was not inside the catalog, as in these cases it is unlikely that there will be another galaxy at a similar redshift to give the posterior support in that location.

D. MDC3: Luminosity Weighting

Until now we have considered all galaxies in our catalog to be equally likely to host a gravitational-wave source. In MDC3 we analyse the case where this is no longer true by constructing a galaxy catalog such that the probability of any single galaxy hosting a GW source was directly proportional to its luminosity. This models the case in which GW events trace the luminosity of galaxies, commonly expected to be true in the real universe, as luminosity can be a tracer for star formation rate (B-band) or galaxy mass (K-band), both of which would logically be correlated with higher rates of GW mergers. MDC3 includes the same EM selection effects as MDC2, in that the catalog is magnitude limited. The completeness of this catalog, defined in terms of luminosity rather

than numbers of galaxies, as defined in Eq. 15, is 50% out to 115 Mpc. This is indicative that approximately 50% of the detected GW events have host galaxies inside the catalog.

To investigate the importance of this effect, MDC3 was analyzed twice under different assumptions, given in Eq. A.2. In the first, the analysis was matched to the known properties of the galaxy catalog, such that the probability of any galaxy hosting a GW event was proportional to its luminosity. In the second, we feigned ignorance and ran the analysis with the assumption that each galaxy was equally likely to be host to a GW event (as was true in MDCs 1 and 2). This allows us to determine the effect of ignoring galaxy weighting with this dataset. The combined H_0 posteriors for both cases are shown in Fig. 7. The estimated values of the Hubble constant are $70.38^{+3.49}_{-2.64}$ $\text{km s}^{-1} \text{Mpc}^{-1}$ (assuming hosts are luminosity weighted) and $68.95^{+4.41}_{-3.54}$ $\text{km s}^{-1} \text{Mpc}^{-1}$ (assuming equal weights). By matching the analysis to the known qualities of the galaxy catalog, using the known luminosity weighting of host galaxies, the constraint on H_0 is improved in that the uncertainty narrows by a factor of 1.3, compared to the case in which equal weights are assumed. Both results are consistent with the fiducial H_0 value of $70 \text{ km s}^{-1} \text{Mpc}^{-1}$. In the limit of a far greater number of events, one might expect to see a bias emerge in the case in which the assumptions in the analysis do not match those with which the catalog was simulated. The luminosity weighting of host galaxies, by its very nature, increases the probability that the host galaxy is inside the galaxy catalog; assuming equal weighting gives disproportionate weight to the contribution that comes from beyond the galaxy catalog. However, for the 249 BNS events considered here, the final posteriors are too broad to be able to detect any kind of bias.

E. Comparison between the MDCs

So far we have focused on individual event likelihoods and combined results for all 249 events. Our data-set also allows us to assess the convergence for the combined Hubble posterior as we add events. We calculate the intermediate combined posteriors as a function of the number of events, and show the resulting convergence in Fig. 8. We plot the fractional H_0 uncertainty (defined here as the width of the 68.3% credible interval divided by H_0 , $\Delta_{H_0}^{68.3\%}/H_0$), against the number of events we include in a randomly-selected group. The scatter between realizations of the group is indicated by the error bars, which encompass 68.3% of their range. There is a considerable variation between different realizations, for the incomplete catalogs. For example, of the 100 realization we used, for 25% completeness and 40 events, there are groups that give $\sim 10\%$ precision, but others that give $\sim 70\%$ precision.

With a sufficiently large number of events, we expect a $1/\sqrt{N}$ scaling of the with the number of events. To check whether this behavior is indeed true, we fit the results for each MDC to the expected scaling, obtaining the coefficient of $1/\sqrt{N}$ by maximizing its likelihood given the fractional uncertainties and their variances from the different realizations.

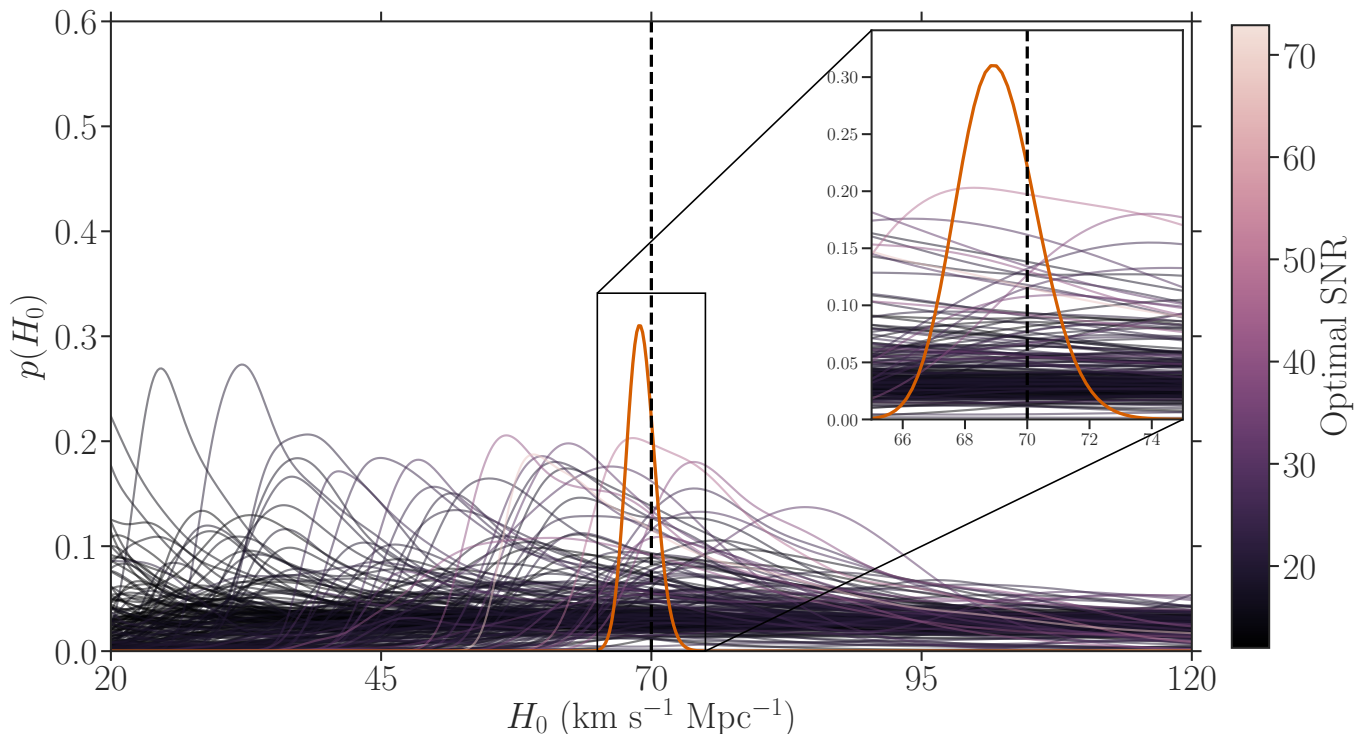


FIG. 4. In orange we show the posterior probability on H_0 for MDC1. We also show the individual likelihoods of all events, color coded according to their optimal SNR and scaled up by an arbitrary value so that details can be seen more easily.

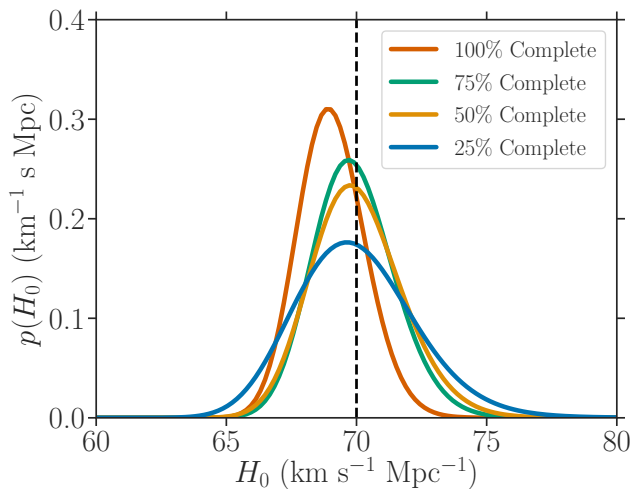


FIG. 5. Posterior probability on H_0 for the mock data challenge where the number completeness of the galaxy catalog varies as a function of the chosen apparent magnitude limits for each catalog. In green, yellow and blue we show the 100%, 75%, 50% and 25% completeness (out to 115 Mpc) cases respectively.

The coefficient of the scaling is automatically dominated by the fractional uncertainties at large N where the variances are small. We show this scaling for each MDC as a set of dashed lines in Fig. 8.

It can be seen that for each MDC the data converges to the expected $1/\sqrt{N}$ scaling. The number of events required before this behavior is reached is dependent on the amount of EM information available on average for each event. The direct counterpart case is always on the trend, after $\mathcal{O}(10)$ events, while even with the most complete galaxy catalogs, if the host galaxy is not directly identified it will take tens of events before this behavior is reached. However, even the least complete catalog (25%) appears to have reached this behavior by the time all 249 events are combined. It should be noted that as the catalogs for MDCs 1 and 2 were not simulated realistically, their low density relative to the density of the universe means that these numbers should not be taken as predictions of how fast $1/\sqrt{N}$ may be reached in real life (except, perhaps, in the counterpart case, though bear in mind that even here peculiar velocities and redshift uncertainties have been neglected). Even with a galaxy catalog which is 25% complete, MDC2 gives a result which is only about a factor of 3 times worse than the counterpart case. These optimistic results are possibly also an artefact of the unrealistic nature of the galaxy catalogs used for these simulations.

As the density of galaxies in MDC3 was increased by 2 orders of magnitude over MDCs 1 and 2, the final posteriors cannot be directly compared between MDCs. However, by plotting the equivalent convergence figure for MDC3 (including the “known host” case as a reference, see Fig. 8), one can see the impact of increasing the density of galaxies in the universe on the speed at which the posterior converges on the $1/\sqrt{N}$ behavior. As there are more host galaxies, the results

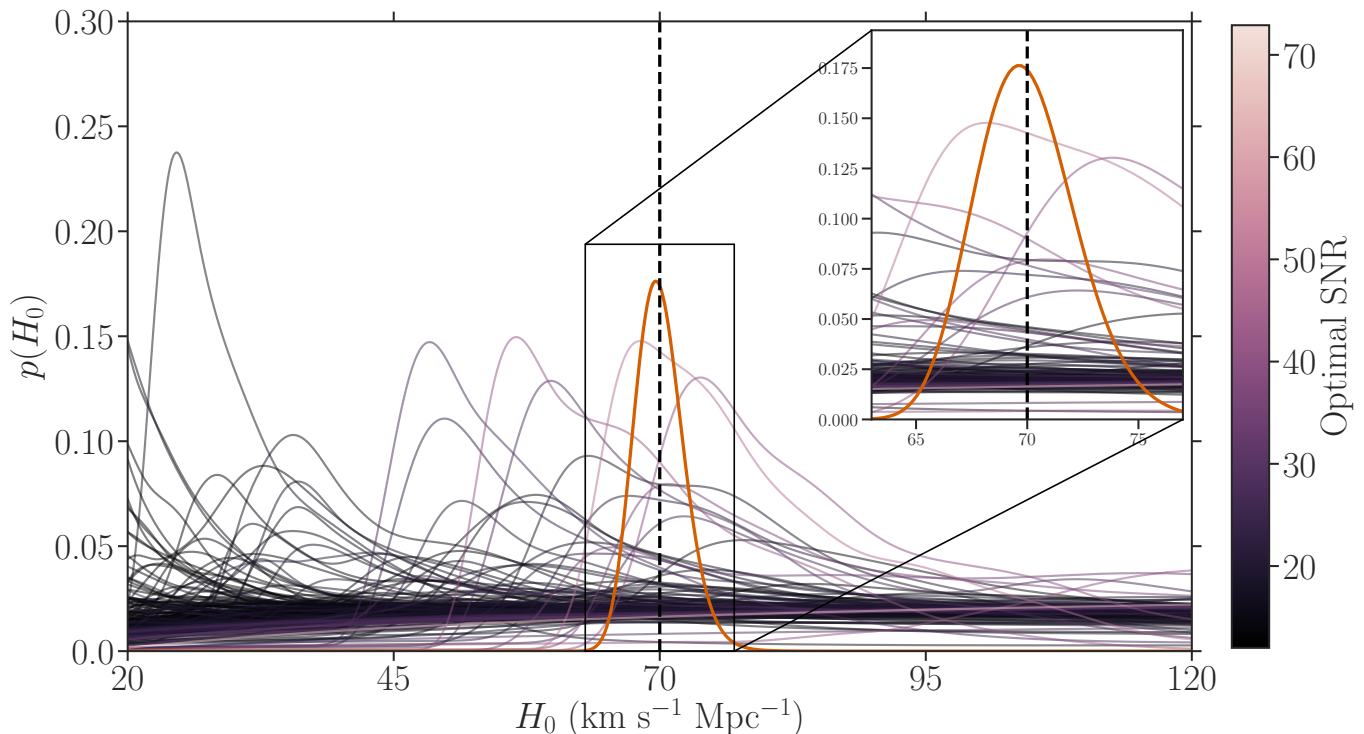


FIG. 6. Likelihoods (purple shades representing optimal SNR) and combined posterior (orange) for a 25% complete galaxy catalog (see IV C). Compared to figs 2 and 4 fewer individual likelihoods are peaked, and the H_0 estimate is a less precise $69.64^{+2.44}_{-2.10}$ $\text{km s}^{-1} \text{Mpc}^{-1}$.

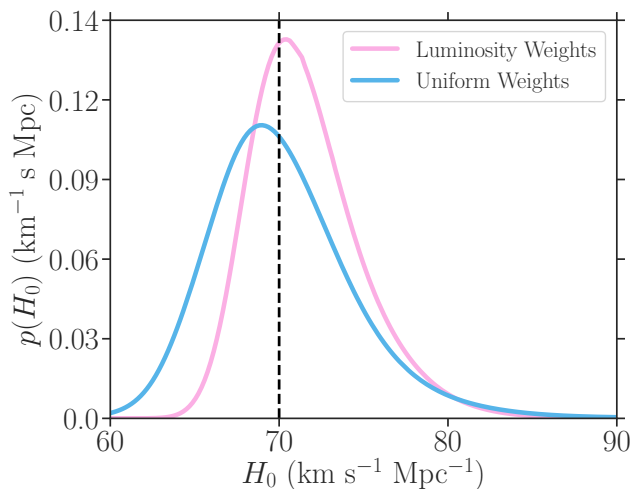


FIG. 7. Posterior probability on H_0 for MDC3. By construction, the probability of any galaxy hosting a GW event is proportional to its luminosity. The pink curve gives the posterior for the case where we take this luminosity weighting into account in our analysis. The blue curve gives the posterior for the case where we ignore this extra information, and treat every galaxy as equally likely to be hosts.

are overall less precise, and take longer to reach the $1/\sqrt{N}$ trend indicating a convergence on a Gaussian posterior. As expected, using luminosity-weighting of potential host galax-

ies as a assumption in the analysis concentrates the probability in a smaller number of galaxies, leading to a more precise result.

F. Limited Robustness Studies

Our results are expected to be sensitive to the luminosity distribution parameters — if one uses values of the Schechter function parameters α and L^* in the analysis which are different from the ones used to simulate the galaxy catalogs, one would expect to end up with a bias in the results. With variations of these parameters within their current measurement uncertainties, we have however demonstrated that the resulting variation in the final result is small compared to the statistical uncertainties reached with the current set of MDCs. Furthermore we have also demonstrated that our results are robust against a small $O(1)$ variation in the value of the telescope sensitivity threshold m_{th} .

V. CONCLUSIONS AND OUTLOOK

H_0 measurement with gravitational waves has been demonstrated with recent events, including both the counterpart method for GW170817 [7], and the galaxy catalogue method [10, 11]. These approaches are combined in the analysis of both BNS and BBH events from the first two observing runs of the advanced detector network [12], using the method

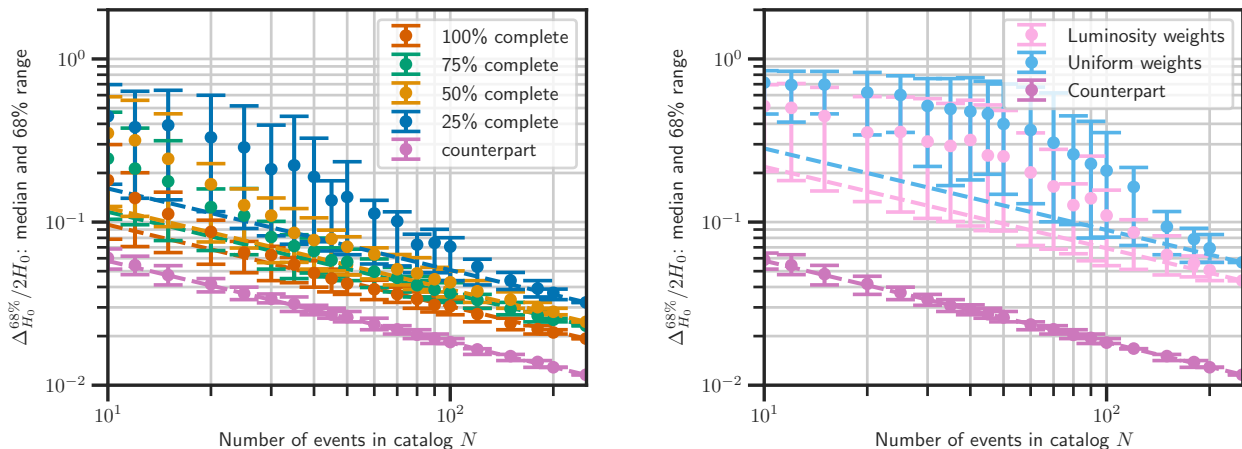


FIG. 8. Fractional uncertainty in H_0 as a function of the number N of the events for the combined H_0 posteriors. The fractional uncertainty in H_0 is defined as the width of the 68.3% highest probability interval divided by $70 \text{ km s}^{-1} \text{ Mpc}^{-1}$, and is shown as the plotted dots for all cases. (left) In purple, red, green, yellow and blue we show the associated host galaxy case (MDC0), complete galaxy catalog (MDC1) case, and the 75%, 50% and 25% completeness cases; we find a fractional H_0 uncertainty of 1.13%, 1.84%, 2.21%, 2.46% and 3.24% respectively for the combined H_0 posterior from 249 events. (right) convergence for MDC3 (event probability proportional to galaxy luminosity), analyzed with luminosity-weighted likelihood (pink) or equally-weighted likelihood (light blue). We find fractional H_0 uncertainties of 4.38% and 5.68% respectively. MDC0 (purple) is included for reference. We plot the expected $1/\sqrt{N}$ scaling behavior for large values of N for all cases with the dashed lines. This scaling behavior is met by all MDCs as the number of events reaches 249, but for the less informative, lower completeness MDCs the trend is slower to emerge. This is even more evident in MDC3, where the density of galaxies is 100 times greater, producing more potential hosts for each event. This is mitigated somewhat by the effect of luminosity-weighting the potential hosts (pink).

described in this paper. Future measurements will rely on a combination of counterpart and catalog methods, as appropriate for each new detected event, with catalog incompleteness playing an important role for the more distant, yet more common, BBHs. This paper outlines a coherent approach that tackles both of these scenarios, including treatment of selection effects in both GWs (due to the limited sensitivity of GW detectors) and EM (due to the flux-limitations of EM observing channels). We performed a series of MDCs to validate our method using up to 249 observed events. For each of the MDCs analyzed, the final posterior on H_0 is found to be consistent with the value of $H_0 = 70 \text{ km s}^{-1} \text{ Mpc}^{-1}$ used to simulate the MDC galaxy catalogs, demonstrating that our method can produce sufficiently unbiased results for treating these numbers of events, in our simulations.

GW selection effects are inherent in every version of the MDC and were corrected for by the term $p(D_{\text{GW}}|H_0)$ in the denominator of Eq. (6). EM selection effects are addressed in MDCs 2 and 3 by the out-of-catalog terms containing \bar{G} in Eq. (8). In both these MDCs, in spite of having an apparent magnitude-limited galaxy catalog, we are able to accurately infer H_0 without any bias. MDC2 further demonstrates our ability to account for missing host galaxies down to a level where only 25% of events have hosts inside the catalog. Even in this case, we converge to the correct H_0 value, to the level of precision which could be reached by 249 events.

MDC3 demonstrates a clear tightening of the posterior distribution when we can assume that GW events trace the galaxy luminosities, compared to the case in which we treat all galax-

ies as equally likely hosts. The equal weights analysis of this MDC remains consistent with the injected H_0 value, leaving us unable to conclude whether an incorrect assumption would lead to a biased result, as one might expect. Since for 249 BNS events, both analyses remain consistent, and it is only with a much greater number of events that any underlying bias would be detected. Future work will be needed to expand these studies to include much greater numbers of GW events.

Although the statistical standard siren measurement of H_0 is less precise than the counterpart measurement, it appears that the galaxy catalog method is still able to accurately constrain H_0 without any counterpart at all, although at least an order of magnitude more events is required to reach comparable accuracy (in the most realistic case of MDC3). While these MDCs have validated our method and implementation in simplified scenarios, future work can improve on this in several directions that are required for treatment of sources such as BBHs out to farther distances, realistic cosmology, and real galaxy catalogs [12]. In particular, the lack of redshift uncertainties and peculiar velocities means that the contributions from individual galaxies are a lot more precise here than they would be in reality, where their uncertainties would propagate to the final result. Moreover, the simulated catalogs in MDCs 1 and 2 had a low density of galaxies compared to the Universe, making them more informative than real catalogs. MDC3, with a galaxy density of 1 galaxy per 70 Mpc^3 , comes closest to the actual density of galaxies in the local universe of ~ 1 galaxy per 200 Mpc^3 [30]. In this scenario there is still a clear convergence towards the injected H_0 value. In

comparison to actual catalogs such as GLADE [30], the apparent magnitude threshold of 14 is very low, so we expect a real catalog-only analysis to fall somewhere between MDCs 2 and 3. However, we caution that with tens of events, results can vary by almost an order of magnitude depending on the particular realisation of the detected population, before eventually converging to the expected $1/\sqrt{N}$ behaviour. Analysing more realistic catalogs also requires a sky-varying EM selection function, as the magnitude threshold varies significantly on the sky according to the design of particular surveys.

The galaxy distribution in these simulated catalogs is uniform in comoving volume. Although it has not been studied here, clustering of galaxies is expected to improve the constraint on H_0 (see, *e.g.* [13]), since even when the host is not in the catalog, it is likely that there will be observed galaxies nearby.

The Advanced LIGO - Virgo second observing run [9] has confirmed that BBH systems are detected at higher rates than BNSs. Since their greater mass allows them to be observed at much greater distances, where galaxy catalogs are incomplete, the catalog method including EM selection effects is particularly important. Additional information may be forthcoming once their population can be accurately inferred, particularly from the mass distribution and rate of events, although caution must be taken as both these quantities are expected to evolve with redshift [22, 24]. With the catalog of GW events expected to expand at an increasing rate in future observing

runs, our analysis will evolve to meet these requirements and give us the fullest picture of cosmology as revealed by gravitational waves.

ACKNOWLEDGMENTS

We thank members of the LIGO-Virgo Collaboration for valuable discussions pertaining to the writing of this paper, and in particular Nicola Tamanini for a careful reading of the manuscript. AG thanks P. Ajith, Walter Del Pozzo, Anuradha Samajdar, and Chris Van Den Broeck for discussion at various stages of the work. IMH is supported by the NSF Graduate Research Fellowship Program under grant DGE-17247915. IMH also acknowledges support from NSF Award PHY-1607585. AS thanks Nikhef for its hospitality and support from the Amsterdam Excellence Scholarship (2016-2018). HYC was supported by the Black Hole Initiative at Harvard University, through a grant from the John Templeton Foundation. AG is supported by the research programme of the Netherlands Organisation for Scientific Research (NWO). CM is supported by the Science and Technology Research Council (grant No.ST/L000946/1). We are grateful for computational resources provided by the Leonard E Parker Center for Gravitation, Cosmology and Astrophysics at the University of Wisconsin-Milwaukee, and that provided by Cardiff University, and funded by an STFC grant supporting UK Involvement in the Operation of Advanced LIGO.

-
- [1] B. F. Schutz, *Nature (London)* **323**, 310 (1986).
 - [2] N. Aghanim *et al.* (Planck), (2018), arXiv:1807.06209 [astro-ph.CO].
 - [3] A. G. Riess, S. Casertano, W. Yuan, L. M. Macri, and D. Scolnic, *Astrophys. J.* **876**, 85 (2019), arXiv:1903.07603 [astro-ph.CO].
 - [4] B. P. Abbott, R. Abbott, T. D. Abbott, F. Acernese, K. Ackley, C. Adams, T. Adams, P. Addesso, and et al. (LIGO Scientific Collaboration and Virgo Collaboration), *Phys. Rev. Lett.* **119**, 161101 (2017).
 - [5] B. P. Abbott, R. Abbott, T. D. Abbott, F. Acernese, K. Ackley, C. Adams, T. Adams, P. Addesso, and et al., *ApJ* **848**, L12 (2017).
 - [6] M. Soares-Santos, D. E. Holz, J. Annis, R. Chornock, K. Herner, Berger, and et al., *ApJL* **848**, L16 (2017).
 - [7] B. P. Abbott, R. Abbott, T. D. Abbott, F. Acernese, K. Ackley, C. Adams, T. Adams, P. Addesso, and et al. (LIGO Scientific Collaboration and Virgo Collaboration), *Nature (London)* **551**, 85 (2017), arXiv:1710.05835.
 - [8] W. Del Pozzo, *Phys. Rev. D* **86**, 043011 (2012), arXiv:1108.1317.
 - [9] B. P. Abbott *et al.* (LIGO Scientific, Virgo), (2018), arXiv:1811.12907 [astro-ph.HE].
 - [10] M. Fishbach *et al.* (LIGO Scientific, Virgo), *Astrophys. J.* **871**, L13 (2019), arXiv:1807.05667 [astro-ph.CO].
 - [11] M. Soares-Santos *et al.* (DES, LIGO Scientific, Virgo), *Astrophys. J.* **876**, L7 (2019), arXiv:1901.01540 [astro-ph.CO].
 - [12] LVC, <https://dcc.ligo.org/LIGO-P1900015> **TBD** (2019).
 - [13] H.-Y. Chen, M. Fishbach, and D. E. Holz, *Nature* **562**, 545 (2018), arXiv:1712.06531 [astro-ph.CO].
 - [14] B. P. Abbott, R. Abbott, T. D. Abbott, M. R. Abernathy, F. Acernese, K. Ackley, C. Adams, T. Adams, P. Addesso, and R. X. Adhikari, *Living Reviews in Relativity* **21**, 3 (2018), arXiv:1304.0670 [gr-qc].
 - [15] D. Castelvecchi, *Nature (London)* **565**, 9 (2019).
 - [16] T. Padma, *Nature (London)* (2019), 10.1038/d41586-019-00184-z.
 - [17] B. P. Abbott *et al.* (LIGO Scientific, Virgo), (2018), arXiv:1811.12940 [astro-ph.HE].
 - [18] B. P. Abbott, R. Abbott, T. D. Abbott, S. Abraham, F. Acernese, K. Ackley, C. Adams, R. X. Adhikari, V. B. Adya, and C. Affeldt, *Astrophys. J.* **875**, 161 (2019), arXiv:1901.03310 [astro-ph.HE].
 - [19] S. Nissanke, D. E. Holz, N. Dalal, S. A. Hughes, J. L. Sievers, and C. M. Hirata, (2013), arXiv:1307.2638 [astro-ph.CO].
 - [20] D. W. Hogg, (1999), arXiv:astro-ph/9905116 [astro-ph].
 - [21] B. S. Sathyaprakash and B. F. Schutz, *Living Rev. Rel.* **12**, 2 (2009), arXiv:0903.0338 [gr-qc].
 - [22] S. R. Taylor, J. R. Gair, and I. Mandel, *Phys. Rev. D* **85**, 023535 (2012), arXiv:1108.5161 [gr-qc].
 - [23] C. Messenger and J. Read, *Phys. Rev. Lett.* **108**, 091101 (2012), arXiv:1107.5725 [gr-qc].
 - [24] M. Fishbach, D. E. Holz, and W. M. Farr, *Astrophys. J.* **863**, L41 (2018), [Astrophys. J. Lett.863,L41(2018)], arXiv:1805.10270 [astro-ph.HE].
 - [25] L. P. Singer, L. R. Price, B. Farr, A. L. Urban, C. Pankow, S. Vitale, J. Veitch, W. M. Farr, C. Hanna, K. Cannon, T. Downes,

- P. Graff, C.-J. Haster, I. Mandel, T. Sidery, and A. Vecchio, *Astrophys. J.* **795**, 105 (2014), arXiv:1404.5623 [astro-ph.HE].
- [26] C. P. L. Berry *et al.*, *Astrophys. J.* **804**, 114 (2015), arXiv:1411.6934 [astro-ph.HE].
- [27] C. Messick, K. Blackburn, P. Brady, P. Brockill, K. Cannon, R. Cariou, S. Caudill, S. J. Chamberlin, J. D. E. Creighton, R. Everett, C. Hanna, D. Keppel, R. N. Lang, T. G. F. Li, D. Meacher, A. Nielsen, C. Pankow, S. Privitera, H. Qi, S. Sachdev, L. Sadeghian, L. Singer, E. G. Thomas, L. Wade, M. Wade, A. Weinstein, and K. Wiesner, *Phys. Rev. D* **95**, 042001 (2017), arXiv:1604.04324 [astro-ph.IM].
- [28] J. Veitch, V. Raymond, B. Farr, W. Farr, P. Graff, S. Vitale, B. Aylott, K. Blackburn, N. Christensen, M. Coughlin, W. Del Pozzo, F. Feroz, J. Gair, C.-J. Haster, V. Kalogera, T. Littenberg, I. Mandel, R. O’Shaughnessy, M. Pitkin, C. Rodriguez, C. Röver, T. Sidery, R. Smith, M. Van Der Sluys, A. Vecchio, W. Vousden, and L. Wade, *Phys. Rev. D* **91**, 042003 (2015), arXiv:1409.7215 [gr-qc].
- [29] W. Del Pozzo, C. P. Berry, A. Ghosh, T. S. F. Haines, L. P. Singer, and A. Vecchio, *Mon. Not. Roy. Astron. Soc.* **479**, 601 (2018), arXiv:1801.08009 [astro-ph.IM].
- [30] G. Dálya, G. Galgóczi, L. Dobos, Z. Frei, I. S. Heng, R. Macas, C. Messenger, P. Raffai, and R. S. de Souza, *Mon. Not. Roy. Astron. Soc.* **479**, 2374 (2018), arXiv:1804.05709 [astro-ph.HE].
- [31] J. Binney and S. Tremaine, “Galactic dynamics,” (Princeton University Press, 1987) Chap. 1, pp. 21–22.

Appendix: Detailed methodology

1. A note on luminosity weighting and redshift evolution

Whenever there is ambiguity about the host of a GW event, we must consider that certain properties of the galaxies may give them different probabilities of hosting the event. More luminous galaxies are more likely to host GW mergers, if they are biased tracers for the overall stellar mass of the galaxies or their star-formation rate. Galaxies at higher redshifts may be more likely to be hosts, as mergers are expected to be more common further back in time.

When considering the terms x_{GW} and D_{GW} we have made the implicit assumption that a real gravitational wave event has been detected, and it is not a false alarm. To make the discussion that follows formal, let us denote by s the fact that there was a GW source. For most of the time, the term s is not important, and it only becomes important when considering which properties of the galaxies the mergers trace.

More precisely, when we consider our priors on the galaxy distribution in the universe (denoted in later sections as $p(z, \Omega, M, m|H_0)$), we recognize that what we are actually interested is the prior on host galaxies for GW events denoted by the conditional probability $p(z, \Omega, M, m|s, H_0)$. For the general case, we assume z , Ω and M to be independent, while m is a function of z , M and H_0 . We calculate this probability as follows,

$$\begin{aligned}
 p(z, \Omega, M, m|s, H_0) &= p(m|z, \Omega, M, s, H_0)p(z, \Omega, M|s, H_0), \\
 &= \delta(m - m(z, M, H_0))p(z|s, H_0)p(\Omega|s, H_0)p(M|s, H_0), \\
 &= \delta(m - m(z, M, H_0))p(z|s)p(\Omega)p(M|s, H_0), \\
 &= \frac{1}{p(s)p(s|H_0)}\delta(m - m(z, M, H_0))p(s|z)p(z)p(\Omega)p(s|M, H_0)p(M|H_0),
 \end{aligned} \tag{A.1}$$

where in the last line we make use of the explicit functional relation between apparent magnitudes as function of z , M and H_0 . Here, $p(z)$ is the prior distribution of galaxies in the universe, taken to be uniform in comoving volume-time⁸, $p(\Omega)$ is the prior on galaxy sky location, taken to be uniform across the sky, and $p(M|H_0)$ is the distribution of absolute magnitudes represented by the Schechter function. In the sections below it will be seen that the terms $p(s)$ and $p(s|H_0)$ cancel in the numerator and denominator of each term for which they appear, and so their exact form does not need to be considered.

If we believe that the probability of a given galaxy being a host to the gravitational wave source is dependent on the galaxy’s absolute magnitude, then $p(s|M, H_0)$ takes some non-constant value:

$$p(s|M, H_0) \propto \begin{cases} L(M(H_0)), & \text{if weights } \propto \text{luminosity} \\ \text{constant} & \text{if weights are uniform.} \end{cases} \tag{A.2}$$

The above relation is what we refer to as luminosity weighting throughout the paper.

The term $p(s|z)$ can be interpreted as how the merger rate depends on redshift,

$$p(s|z) \propto \begin{cases} \text{function}(z) & \text{if rate evolves with redshift} \\ \text{constant} & \text{if rate does not evolve with redshift.} \end{cases} \tag{A.3}$$

⁸ Comoving volume-time, as opposed to comoving volume, in order to take

into account the delay due to the travel time of any emitted signals.

For the MDCs in this paper with $z \ll 1$, a non-trivial evolution of merger rate on redshift is not expected to make any difference in the results, and we assume a constant rate model. A more generic model with $p(s|z) \propto (1+z)^l$ can be used as we go to farther redshifts. In [12], for example, this methodology has been used with constant as well as $p(s|z) \propto (1+z)^3$ rate models in order to test the robustness of the results there against a variation on the assumptions on the merger rate.

2. Individual components of the statistical case

Now we consider the individual components of Eq. 8 and provide explicit expressions for each. Note that in the cases where the integration limits are not specified, they can be assumed to cover the full parameter space. We explicitly include s , denoting “a source is present”, for clarity.

a. *Likelihood when host is in catalog:* $p(x_{\text{GW}}|G, D_{\text{GW}}, H_0)$

First expanding as in Eq. 6:

$$p(x_{\text{GW}}|G, D_{\text{GW}}, s, H_0) = \frac{p(x_{\text{GW}}|G, s, H_0)}{p(D_{\text{GW}}|G, s, H_0)}. \quad (\text{A.4})$$

We find the numerator by marginalizing over redshift, sky location, absolute magnitude and apparent magnitude:

$$\begin{aligned} p(x_{\text{GW}}|G, s, H_0) &= \iiint p(x_{\text{GW}}|z, \Omega, M, m, G, s, H_0) p(z, \Omega, M, m|G, s, H_0) dz d\Omega dM dm, \\ &= \iiint p(x_{\text{GW}}|z, \Omega, s, H_0) p(z, \Omega, M, m|G, s, H_0) dz d\Omega dM dm, \end{aligned} \quad (\text{A.5})$$

which is true if we can assume that x_{GW} is independent of G , m and M .

The dependence of the priors on G means that we take $p(z, \Omega, M, m|G, s, H_0)$ as a sum of delta functions with specific z , Ω and m corresponding to the location of each galaxy in the catalog. Because the values of z , Ω , m and M are related through the specific galaxies inside the catalog, the expansion differs to that shown in section 1.

$$\begin{aligned} p(z, \Omega, M, m|G, s, H_0) &= \frac{p(s|z, \Omega, M, m, G, H_0) p(z, \Omega, M, m|G, H_0)}{p(s|G, H_0)}, \\ &= \frac{p(s|z, \Omega, M, m, G, H_0) p(M|z, \Omega, m, G, H_0) p(z, \Omega, m|H_0, G)}{p(s|G, H_0)}, \\ &= \frac{p(s|z, \Omega, M, m, G, H_0) \delta(M - M(z, m, H_0)) p(z, \Omega, m|G)}{p(s|G, H_0)}. \end{aligned} \quad (\text{A.6})$$

Substituting this back into the equation above and integrating over M gives,

$$p(x_{\text{GW}}|G, s, H_0) = \frac{1}{p(s|G, H_0)} \iiint p(x_{\text{GW}}|z, \Omega, s, H_0) p(s|z, \Omega, M(z, m, H_0), m, G, H_0) p(z, \Omega, m|G) dz d\Omega dm. \quad (\text{A.7})$$

Now explicitly changing the integral to a sum over N galaxies within the galaxy catalog, distributed as $p(z, \Omega, m|G)$:

$$\begin{aligned} p(x_{\text{GW}}|G, s, H_0) &= \frac{1}{p(s|G, H_0)} \frac{1}{N} \sum_{i=1}^N p(x_{\text{GW}}|z_i, \Omega_i, s, H_0) p(s|z_i, \Omega_i, M(z_i, m_i, H_0), m_i, H_0), \\ &= \frac{1}{p(s|G, H_0)} \frac{1}{N} \sum_{i=1}^N p(x_{\text{GW}}|z_i, \Omega_i, s, H_0) p(s|z_i, M(z_i, m_i, H_0)), \\ &= \frac{1}{p(s|G, H_0)} \frac{1}{N} \sum_{i=1}^N p(x_{\text{GW}}|z_i, \Omega_i, s, H_0) \frac{p(z_i, M(z_i, m_i, H_0)|s) p(s)}{p(z_i, M(z_i, m_i, H_0))}, \\ &= \frac{1}{p(s|G, H_0)} \frac{1}{N} \sum_{i=1}^N p(x_{\text{GW}}|z_i, \Omega_i, s, H_0) \frac{p(z_i|s) p(M(z_i, m_i, H_0)|s) p(s)}{p(z_i) p(M(z_i, m_i, H_0))}. \end{aligned} \quad (\text{A.8})$$

Expanding $p(z_i|s)$ and $p(M(z_i, m_i, H_0)|s)$, and noting that some terms cancel leads to

$$p(x_{\text{GW}}|G, s, H_0) = \frac{1}{p(s)p(s|G, H_0)} \frac{1}{N} \sum_{i=1}^N p(x_{\text{GW}}|z_i, \Omega_i, s, H_0)p(s|z_i)p(s|M(z_i, m_i, H_0)). \quad (\text{A.9})$$

Expanding the denominator, $p(D_{\text{GW}}|G, s, H_0)$, in the same way, then substituting both back into Eq A.4, the factors out front cancel, and the expression becomes:

$$p(x_{\text{GW}}|G, D_{\text{GW}}, s, H_0) = \frac{\sum_{i=1}^N p(x_{\text{GW}}|z_i, \Omega_i, s, H_0)p(s|z_i)p(s|M(z_i, m_i, H_0))}{\sum_{i=1}^N p(D_{\text{GW}}|z_i, \Omega_i, s, H_0)p(s|z_i)p(s|M(z_i, m_i, H_0))}. \quad (\text{A.10})$$

If we consider the (realistic) case in which galaxies are point sources in Ω , but have some associated z error, we can take this uncertainty into account by integrating over the redshift distribution of each galaxy, $p(z_i)$:

$$p(x_{\text{GW}}|G, D_{\text{GW}}, s, H_0) = \frac{\sum_{i=1}^{N_{\text{gal}}} \int p(x_{\text{GW}}|z_i, \Omega_i, s, H_0)p(s|z_i)p(s|M(z_i, m_i, H_0))p(z_i)dz_i}{\sum_{i=1}^{N_{\text{gal}}} \int p(D_{\text{GW}}|z_i, \Omega_i, s, H_0)p(s|z_i)p(s|M(z_i, m_i, H_0))p(z_i)dz_i}. \quad (\text{A.11})$$

b. Probability the host galaxy is in the galaxy catalog: $p(G|D_{\text{GW}}, H_0)$

The probability that the host galaxy is within the galaxy catalog is given by,

$$\begin{aligned} p(G|D_{\text{GW}}, s, H_0) &= \iiint p(G|z, \Omega, M, m, D_{\text{GW}}, s, H_0)p(z, \Omega, M, m|D_{\text{GW}}, s, H_0)dzd\Omega dM dm, \\ &= \iiint \Theta[m_{\text{th}} - m] \frac{p(D_{\text{GW}}|z, \Omega, M, m, s, H_0)p(z, \Omega, M, m|s, H_0)}{p(D_{\text{GW}}|s, H_0)} dzd\Omega dM dm, \\ &= \frac{1}{p(D_{\text{GW}}|s, H_0)} \iiint \Theta[m_{\text{th}} - m] p(D_{\text{GW}}|z, \Omega, s, H_0)p(z, \Omega, M, m|s, H_0) dzd\Omega dM dm. \end{aligned} \quad (\text{A.12})$$

Here $p(G|z, \Omega, M, m, D_{\text{GW}}, s, H_0)$ becomes a Heaviside step function around $m = m_{\text{th}}$, the apparent magnitude threshold of the galaxy catalog⁹.

Expanding $p(z, \Omega, M, m|s, H_0)$ as in Eq A.1, and substituting this into Eq A.12, then utilizing the properties of the delta-function, and Heaviside step function gives:

$$p(G|D_{\text{GW}}, s, H_0) = \frac{1}{p(s)p(s|H_0)} \frac{1}{p(D_{\text{GW}}|s, H_0)} \int_0^{z(M, m_{\text{th}}, H_0)} dz \int d\Omega \int dM p(D_{\text{GW}}|z, \Omega, s, H_0)p(s|z)p(z)p(\Omega)p(s|M, H_0)p(M|H_0). \quad (\text{A.13})$$

The term $p(D_{\text{GW}}|s, H_0)$ can be expanded in a similar way, to give,

$$p(D_{\text{GW}}|s, H_0) = \frac{1}{p(s)p(s|H_0)} \iiint p(D_{\text{GW}}|z, \Omega, s, H_0)p(s|z)p(z)p(\Omega)p(s|M, H_0)p(M|H_0)dzd\Omega dM. \quad (\text{A.14})$$

Substituting this back into Eq A.13 gives,

$$p(G|D_{\text{GW}}, s, H_0) = \frac{\int_0^{z(M, m_{\text{th}}, H_0)} dz \int d\Omega \int dM p(D_{\text{GW}}|z, \Omega, s, H_0)p(s|z)p(z)p(\Omega)p(s|M, H_0)p(M|H_0)}{\iiint p(D_{\text{GW}}|z, \Omega, s, H_0)p(s|z)p(z)p(\Omega)p(s|M, H_0)p(M|H_0)dzd\Omega dM}. \quad (\text{A.15})$$

As the probabilities of being in the catalog and not in the catalog must add up to one, we have,

$$p(\bar{G}|D_{\text{GW}}, s, H_0) = 1 - p(G|D_{\text{GW}}, s, H_0). \quad (\text{A.16})$$

⁹ Here m_{th} is assumed to be uniform across the sky. In the future this assumption will be replaced by an m_{th} which is allowed to vary over the sky.

c. Likelihood when host is not in catalog: $p(x_{\text{GW}}|\bar{G}, D_{\text{GW}}, H_0)$

First expanding as in Eq. 6:

$$p(x_{\text{GW}}|\bar{G}, D_{\text{GW}}, s, H_0) = \frac{p(x_{\text{GW}}|\bar{G}, s, H_0)}{p(D_{\text{GW}}|\bar{G}, s, H_0)}. \quad (\text{A.17})$$

The numerator can be expanded as follows:

$$\begin{aligned} p(x_{\text{GW}}|\bar{G}, s, H_0) &= \iiint p(x_{\text{GW}}|z, \Omega, M, m, \bar{G}, s, H_0) p(z, \Omega, M, m|\bar{G}, s, H_0) dz d\Omega dM dm, \\ &= \iiint p(x_{\text{GW}}|z, \Omega, s, H_0) p(z, \Omega, M, m|\bar{G}, s, H_0) dz d\Omega dM dm, \\ &= \iiint p(x_{\text{GW}}|z, \Omega, s, H_0) \frac{p(\bar{G}|z, \Omega, M, m, s, H_0) p(z, \Omega, M, m|s, H_0)}{p(\bar{G}|s, H_0)} dz d\Omega dM dm, \\ &= \frac{1}{p(\bar{G}|s, H_0)} \iiint p(x_{\text{GW}}|z, \Omega, s, H_0) \Theta(m - m_{\text{th}}) p(z, \Omega, M, m|s, H_0) dz d\Omega dM dm. \end{aligned} \quad (\text{A.18})$$

The prior term, $p(z, \Omega, M, m|s, H_0)$ can now be expanded as it was in Eq A.1. Substituting this in, and utilizing the properties of the delta function and Heaviside step function as before, gives:

$$p(x_{\text{GW}}|\bar{G}, s, H_0) = \frac{1}{p(s)p(s|H_0)} \frac{1}{p(\bar{G}|s, H_0)} \int_{z(H_0, m_{\text{th}}, M)}^{\infty} dz \int d\Omega \int dM p(x_{\text{GW}}|z, \Omega, s, H_0) p(s|z) p(z) p(\Omega) p(s|M, H_0) p(M|H_0). \quad (\text{A.19})$$

Expanding the denominator, $p(D_{\text{GW}}|\bar{G}, s, H_0)$, in the same way gives an equivalent term,

$$p(D_{\text{GW}}|\bar{G}, s, H_0) = \frac{1}{p(s)p(s|H_0)} \frac{1}{p(\bar{G}|s, H_0)} \int_{z(H_0, m_{\text{th}}, M)}^{\infty} dz \int d\Omega \int dM p(D_{\text{GW}}|z, \Omega, s, H_0) p(s|z) p(z) p(\Omega) p(s|M, H_0) p(M|H_0). \quad (\text{A.20})$$

And substituting this back into Eq A.17 finally gives,

$$p(x_{\text{GW}}|\bar{G}, D_{\text{GW}}, s, H_0) = \frac{\int_{z(M, m_{\text{th}}, H_0)}^{\infty} dz \int d\Omega \int dM p(x_{\text{GW}}|z, \Omega, s, H_0) p(s|z) p(z) p(\Omega) p(s|M, H_0) p(M|H_0)}{\int_{z(M, m_{\text{th}}, H_0)}^{\infty} dz \int d\Omega \int dM p(D_{\text{GW}}|z, \Omega, s, H_0) p(s|z) p(z) p(\Omega) p(s|M, H_0) p(M|H_0)}. \quad (\text{A.21})$$

3. The catalog patch case

While in general the galaxy catalog method was derived in 2 for use with a galaxy catalog which covers the entire sky, a small modification allows the use of catalogs which only cover a patch of sky, as long as the patch can be specified using limits in right ascension and declination. If we represent the sky area covered by the catalog as Ω_{cat} , and the area outside the catalog as Ω_{rest} , such that $\Omega_{\text{cat}} + \Omega_{\text{rest}}$ covers the whole sky, this can be written as follows:

$$\begin{aligned} p(x_{\text{GW}}|D_{\text{GW}}, H_0) &= \int p(x_{\text{GW}}|\Omega, D_{\text{GW}}, H_0) p(\Omega) d\Omega, \\ &= \int^{\Omega_{\text{cat}}} p(x_{\text{GW}}|\Omega, D_{\text{GW}}, H_0) p(\Omega) d\Omega + \int^{\Omega_{\text{rest}}} p(x_{\text{GW}}|\Omega, D_{\text{GW}}, H_0) p(\Omega) d\Omega. \end{aligned} \quad (\text{A.22})$$

The first term is equivalent to the regular galaxy catalog case, but with limits on the integral over Ω , while the second term has no G and \bar{G} terms, and covers the rest of the sky from redshift 0 to ∞ .

4. Direct and Pencil Beam Counterpart Cases

The ‘‘direct’’ method assumes that the counterpart has been unambiguously linked to the host galaxy of the GW event, such that the redshift and sky location of that galaxy can be taken to be that of the GW event with certainty, there is no need to marginalise

over the ‘‘in catalog’’ and ‘‘out of catalog’’ terms. Instead the numerator is calculated by evaluating the GW likelihood at the delta-function location of the counterpart in z and Ω , and the term in the denominator is evaluated as:

$$p(D_{\text{GW}}|H_0) = \iiint p(D_{\text{GW}}|z, \Omega, H_0)p(z)p(\Omega)p(M|H_0)dzd\Omega dM, \quad (\text{A.23})$$

for priors $p(z)$ and $p(\Omega)$ (note that this is independent of galaxy catalog data).

The ‘‘pencil-beam’’ method makes the assumption that while the sky location of the galaxy associated with the counterpart is that of the GW event, we may not make a direct association to a known galaxy but to a set of potential candidate hosts. We can use the EM constrained sky localization and therefore return to the question of whether the host is within or beyond the galaxy catalog. In this case, the likelihood takes the same form as in the statistical case, but evaluated along the line of sight of the candidate counterparts.

5. GW selection effects

Eq. 7 in section II C can be written as:

$$p(D_{\text{GW}}|H_0) = \int p(D_{\text{GW}}|x_{\text{GW}}, H_0)p(x_{\text{GW}}|H_0)dx_{\text{GW}}. \quad (\text{A.24})$$

where $p(D_{\text{GW}}|x_{\text{GW}}, H_0)$ is a binary quantity which is 1 if the SNR of x_{GW} passes ρ_{th} , and 0 otherwise.

As in section 2, $p(D_{\text{GW}}|H_0)$ doesn't appear in the expanded versions of any of the equations, but is itself expanded first, such that the actual quantity we require is $p(D_{\text{GW}}|z, \Omega, H_0)$. Calculating $p(D_{\text{GW}}|z, \Omega, H_0)$ requires integrating over all realizations of GW events (detected and not), for a range of z , Ω and H_0 values, and applying a detection threshold (ρ_{th}) which all events must pass in order to be deemed detected.

Practically, Monte-Carlo integration can be used:

$$p(D_{\text{GW}}|z, \Omega, H_0) = \frac{1}{N_{\text{samples}}} \sum_{i=1}^{N_{\text{samples}}} p(D_{\text{GW}_i}|x_{\text{GW}_i}, z, \Omega, H_0). \quad (\text{A.25})$$

where x_{GW_i} corresponds to an event, the parameters of which have been randomly drawn from the prior distributions of parameters which affect an event's detectability (mass, inclination, polarization, and sky location) and the event's ρ_i is calculated for specific values of z and H_0 .

$$p(D_{\text{GW}_i}|x_{\text{GW}_i}, z, \Omega, H_0) = \begin{cases} 1, & \text{if } \rho > \rho_{th} \\ 0, & \text{otherwise.} \end{cases} \quad (\text{A.26})$$

which gives a smooth function for $p(D_{\text{GW}}|z, \Omega, H_0)$, which drops from 1 to 0 over a range of z , Ω and H_0 values.

a. Prior mass distribution

An event's detectability is dependent on its observed (redshifted) detector-frame mass, M_z , but priors on the mass refer to their source-frame mass. When calculating $p(D|H_0)$ the masses are drawn from the priors on source mass, $p(M_1, M_2)$ and then converted to observed masses through the equation:

$$M_z = (1 + z)M. \quad (\text{A.27})$$

However, when we use GW data in the form of posterior samples, the prior used to generate those is uniform on the redshifted mass, M_z [28]. Due to the way the MDC GW data was generated, with masses chosen on the detector-frame, rather than the source-frame, this was not something which had to be considered. With real GW data, as the redshift is linked directly to H_0 , it is necessary to take into account the redshifting of the masses explicitly.

In general, when calculating $p(D|H_0)$ for BBHs, the primary mass M_1 is drawn from a power-law with slope α , between limits $[a, b] M_\odot$. The secondary mass, M_2 is drawn from a uniform distribution between aM_\odot and M_1 [17], to give (for $\alpha \neq -1$):

$$p(M_1, M_2) = \frac{(\alpha + 1)M_1^\alpha}{bM_\odot^{(\alpha+1)} - aM_\odot^{(\alpha+1)}} \frac{1}{M_1 - aM_\odot}. \quad (\text{A.28})$$

This is related to the the redshifted mass by the Jacobian:

$$\begin{aligned} p(M_{1,z}, M_{2,z}) &= p(M_1, M_2) \left| \frac{\partial(M_1, M_2)}{\partial(M_{1,z}, M_{2,z})} \right|, \\ &= p(M_1, M_2) \left| \frac{1}{(1+z)^2} \right|. \end{aligned} \tag{A.29}$$

Substituting in our expression for $p(M_1, M_2)$:

$$\begin{aligned} p(M_{1,z}, M_{1,z}) &= \frac{(\alpha + 1)M_1^\alpha}{bM_\odot^{(\alpha+1)} - aM_\odot^{(\alpha+1)}} \frac{1}{M_1 - aM_\odot} \frac{1}{(1+z)^2}, \\ &= \frac{(1+z)^2(\alpha + 1)M_{1,z}^\alpha}{bM_{\odot,z}^{(\alpha+1)} - aM_{\odot,z}^{(\alpha+1)}} \frac{1}{M_{1,z} - aM_{\odot,z}} \frac{1}{(1+z)^2}, \\ &= \frac{(\alpha + 1)M_{1,z}^\alpha}{bM_{\odot,z}^{(\alpha+1)} - aM_{\odot,z}^{(\alpha+1)}} \frac{1}{M_{1,z} - aM_{\odot,z}}. \end{aligned} \tag{A.30}$$

The factor of $(1+z)^2$ cancels in the numerator and denominator. As all redshift (and hence H_0) dependence has been removed, no correction is required for the differing priors. For the case in which $\alpha = -1$, it can be shown that all redshift dependence falls out as well, meaning that as long as the prior mass distribution takes the form of a power-law, no prior correction is required. This will not be the case for all mass distributions.
